Instrument Science Report WFC3 2016-14

Supplemental Dither Patterns for WFC3/IR

Jay Anderson
August 30, 2016

ABSTRACT

Dithering provides an important way to recover resolution for the badly undersampled WFC3/IR detector. This document develops a framework for constructing and evaluating sub-pixel dithers. There is often a trade-off between the need to do sub-pixel dithering and the need to mitigate artifacts. We evaluate the previously recommended patterns for 2, 3, 4, 6, and 8 points and come up with additional dither patterns for 3, 5, 6, 7, 8, and 9 points for observations for two cases: for the case where the focus is the central region of the detector and for the case where the entire detector is the focus. All the patterns presented here are too tight to provide any mitigation for blobs.

1. INTRODUCTION

The pixels of the WFC3/IR detector are much larger than the structure in the image of a star on the detector. This means that a single image is unable to capture the full resolution of the telescope. We can recover some of this lost information by shifting the scene by small amounts with respect to the pixel boundaries so that some of the sub-pixel structure can be recovered. This is called dithering, and it has become an indispensible strategy for HST observers. A 2010 ISR by Dahlen, Dressel, and Kalirai provides a comprehensive overview of dithering strategies for WFC3/IR and WFC3/UVIS.

In order to make use of the increased resolution that dithering provides, users need tools to combine dithered datasets into a comprehensive picture of the scene. One such strategy involves using a tool such as `Astrodrizzle` to combine the multiple exposures into a single representation of the astrometric

scene. This is by far the most popular and easiest way to improve the resolution from that of the raw images. Unfortunately, the improvement in resolution achieved by `Astrodrizzle` is more qualitative than quantitative, and it is often hard to use `Astrodrizzle` for high-precision studies of structure in the scene, such as whether a source is resolved, and if so how it can be characterized (i.e., as a double star, or with radial profile and perhaps some ellipticity, etc.).

In order to do such high-precision analyses on drizzled sets of images, it is necessary to have three things: (1) good distortion solutions, (2) accurate transformations between the pixels of each exposure and the reference frame, and (3) reliable PSFs. The Institute is beginning to provide accurate `flt`-based PSFs that can be used in such analyses (see Anderson 2016, ISR-2016-12), so it makes sense to start collecting the image data in a way that can take advantage of the sophisticated analyses that are now becoming possible.

The dither patterns described in the current Instrument Handbook[1] provide a qualitative amelioration of the sampling of the scene for a few simple cases where there are 2, 3, or 4 exposures in a set. But there are no recommendations provided for the more general case of N dithers[2]. It is common to split more than 4 exposures into groups of 1, 2, 3 or 4 dithers with offsets between them to ensure that there will be some well-spaced samplings, but interested and motivated users have been left on their own to devise strategies that achieve better than 2×2 super-sampling. For this reason, we explore some additional options for users who may have between 5 and 9 similar exposures in an orbit and would like to implement a coherent dither pattern so as to enable the fullest possible reconstruction of the scene of interest.

One obvious question worth considering is: "How much dithering is enough?" In other words, at what point is the astrometric scene adequately sampled? There can surely be no structure in the scene that is sharper than the PSF, so it suffices to ask how much structure there is in the PSF. Anderson (2016) used a 4×4 supersampled grid to represent the PSF in WFC3/IR images and found that this model provided too much flexibility. He found that the true structure in the PSF can be modeled with roughly 9 degrees of freedom per pixel, or roughly 3×3 super-sampling. For this reason, here we will explore patterns only up to N_{OBS}=9. For datasets with more than 9 similar exposures, it makes sense to group the exposures into subsets with 9 or fewer exposures per subset.

The document is organized as follows. In Section 2, we will discuss the severe impact that distortion has on our ability to dither consistently across the detector. In Section 3, we compare the observed offsets between images to the commanded POS-TARGs so that we can understand exactly how to instruct the telescope to execute a specific sub-pixel dither pattern. In Section 4, we evaluate the existing dither

---

[1] The WFC3 patterns that are selectable in APT are described and quantified in pixels and POS-TARGs in Appendix C of the WFC3 Instrument Handbook. These patterns use the existing framework of LINE and BOX generic convenience patterns in APT, which can be found in Chapter 8 of the Phase II Proposal Instructions: http://www.stsci.edu/hst/programs/hst/proposing/docs/p2pi.html.)

[2] There is an ISR by Dahlen et al (2010-09) that provides a toolbox for dithering and suggests additional patterns for N=6 and N=8, but it is left to the user to do the onerous the sub-pixel offsets to POS-TARGs, and it is not clear that any users have made use of these patterns.

patterns in terms how they are impacted by distortion. In Section 5, we present a set of "TIGHT" dither patterns that have been optimized to provide good pixel-phase coverage for the entire detector for N_{OBS}=2 to N_{OBS}=9. In order to provide a coherent pattern across the detector, we had to cluster the pointings more tightly than is ideal for mitigation of artifacts and persistence, so users should be aware of these tradeoffs. In Section 6 we present a set of "WIDE" dither patterns for N_{OBS}=2 to N_{OBS}=9 that is optimized for smaller targets. If we focus only the center of the detector, we are able to get both good pixel-phase coverage *and* artifact/persistence mitigation. Finally in Section 7 we describe how these patterns can be combined to achieve dithers for $N_{OBS} > 9$.

2. THE IMPACT OF DISTORTION ON DITHERING

Improving the pixel-phase coverage of a data set is not the only reason to dither. It is also useful to dither in order to mitigate the impact of detector artifacts on the reconstructed image. Unfortunately, when there is a significant amount of non-linear distortion present in a detector, it is not always possible to do both. Therefore, choosing the right dither pattern for a particular science project often involves trade-offs.

The WFC3/IR detector is a made up of 1014×1014 pixels, but it does not cover a square field on the sky. The field it covers is closer to a rectangle, since the *x* and *y* pixel axes have different scales. The reason for this is that it would take additional field-corrector optics (and throughput losses) to remove this distortion via hardware, and designers chose to minimize the number of optical elements and thereby maximize the throughput, thus leaving the distortion for users to deal with. In addition to the linear distortion discussed above, the detector also has non-linear distortions amounting to about 2% of the plate scale (the largest terms being the quadratic ones). These non-linear distortions mean that an offset of 10 pixels at the center of the chip can translate to an offset of 10.2 pixels at the edge of the chip. We explore this further below.

3. CONVERTING DITHERS TO POS-TARGS

The actual dithering of the telescope is done in an undistorted frame, in the V2-V3 telescope plane. This means that when we devise a dither pattern with respect to the detector pixels at the center of the chip, we must translate this into the telescope's natural POS-TARG frame. This involves two steps. The detector-pixel-based frame is distorted, so we must first perform the distortion correction to determine the undistorted offsets. We can then take these undistorted offsets and convert the dithers into POS-TARGs, so that we can command the telescope to execute them. The POS-TARG frame is specified in arcseconds, and it is designed to have its *y* axis aligned closely to that of the detector; that alignment is close, but not perfect.

3.1 STEP 1: CORRECTING FOR DISTORTION

The distortion solution we use of here is different from the official solution in the Instrument Handbook in that it is not designed to map the pixels to the absolute V2-V3 plane, but rather it is designed to map the detector as closely as possible to its own frame in order to facilitate differential-astrometry studies. As such, the correction is zero at the center of the chip [507,507] and the frame is scaled and oriented to preserve the direction and scale of the raw detector's *y* axis. The distortion solution thus tells us where each of the detector's pixel is located with respect to the central pixel.

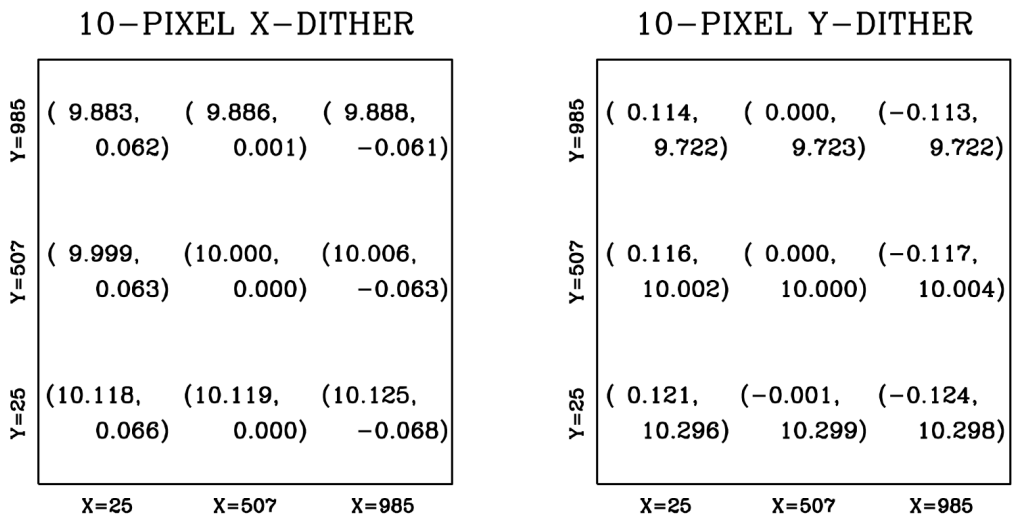

Figure 1: The dithers achieved at various places on the detector for a 10-pixel dither in x (left) and y (right).

We provide this solution in terms of a multi-extension `fits` image that is available and documented at http://www.stsci.edu/hst/wfc3/analysis/PSF. The distortion solution converts from the raw detector coordinates (x,y) to the distortion-corrected coordinates (u,v) If we specify a dither in terms of a $(\Delta x, \Delta y)$ offset at the center of the detector, say from location $(x_1,y_1) = (507.00, 507.00)$ to $(x_2,y_2) = (510.5,507.0)$, we must convert both positions into the distortion-corrected frame and find $(\Delta u, \Delta v) = (u_2\text{-}u_1, v_2\text{-}v_1)$.

Because of distortion, a given dither in the $(\Delta u, \Delta v)$ plane can result in one $(\Delta x, \Delta y)$ offset at the center of the detector, and a different offset in other parts of the detector. The left panel of Figure 1 shows the impact of a 10-pixel dither along the *x* axis. To construct this array of offsets, we determined the $(\Delta u, \Delta v)$ that resulted in a 10-pixel offset at the center of the chip, from raw-detector coordinate (507,507) to raw detector coordinate (517,507). We then took (say) a raw position in the lower-left corner (25.00, 25.00) and found its distortion-corrected-frame location to be (−27.7932, 33.5927) and added to this the $(\Delta u, \Delta v)$ found above to get the location of the second point in the distortion-corrected frame. We then take the inverse distortion correction of this position and subtract (25.00, 25.00) to get the corresponding offset in detector pixel space. We did this for eight points at the edges and corners of the detector and the results are reported in Figure 1.

It is clear that even with a small 10-pixel dither in *x*, the pixel phases achieved can differ by more than 0.15 pixel at the corners. Dithering along the *y* axis introduces an even larger discrepancy: up to 0.3

pixel at the corners. We will make use below of the fact that dithering along the *x* axis introduces perhaps less pixel-phase decoherence than dithering along the *y* axis.

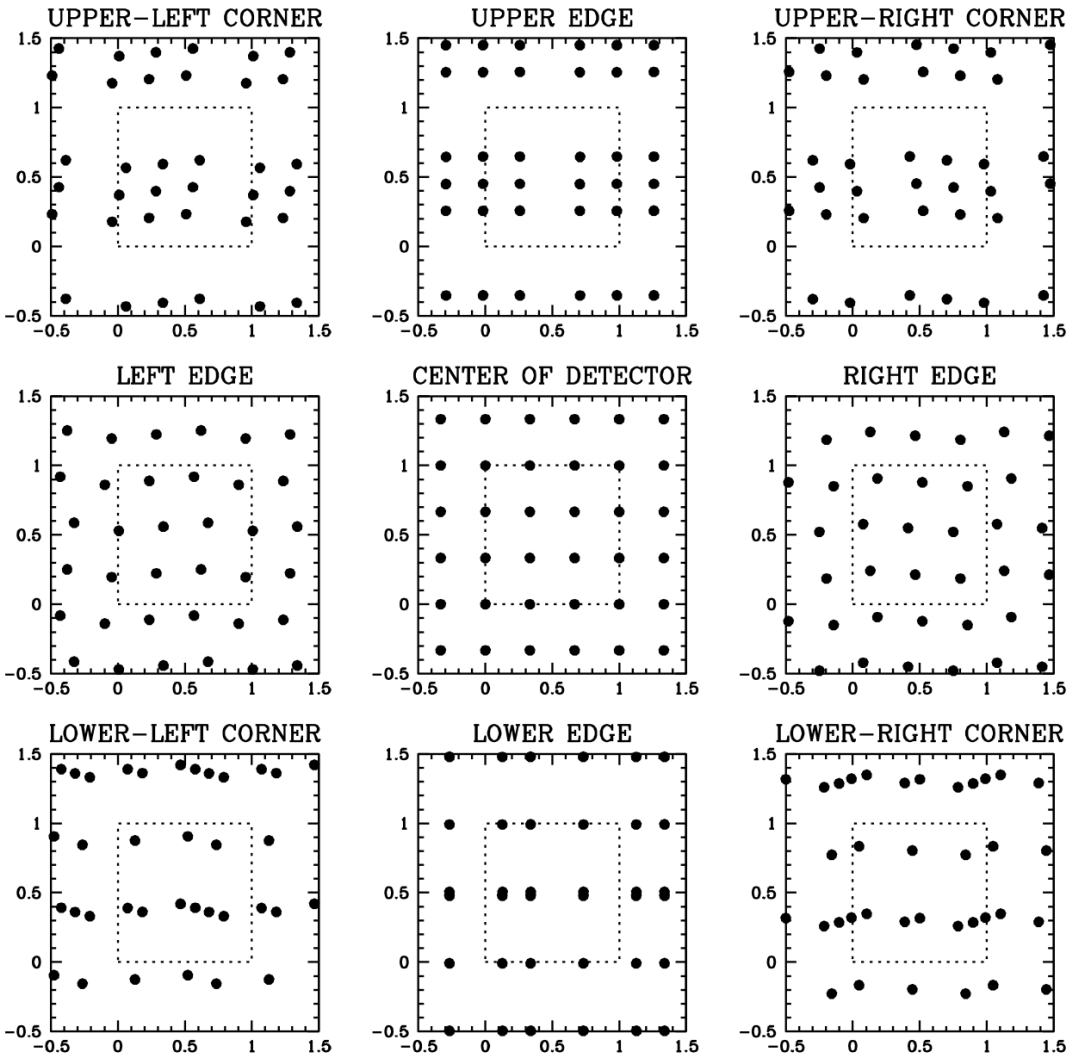

Figure 2: Pixel-phase coverage achieved by a 3×3 array of dithers covering 10×10 image pixels at various locations across the chip. The dotted square shows the outline of a pixel. We show a larger region than just one pixel to give a sense of where the all the samplings are in the case where we wish to reconstruct a scene.

Figure 2 shows the impact of distortion on a 9-point dither in a 3×3 pattern spanning 10×10 detector pixels. The pattern achieves perfect 3×3 super-sampling at the center of the detector (by construction), but distortion causes the pixel-phase sampling to become extremely uneven at the top and bottom of the detector.

Since most of the non-linear distortion is in the quadratic terms, this pixel-phase decoherence scales linearly with the total dither offset, so that smaller dithers will suffer less pixel-phase slippage. In addition, the pixel-phase error is linear with distance from the center of the chip, so that if a target is smaller than full-chip, then one can afford a larger dither before compromising the achieved pixel-phase sampling.

3.2 STEP 2: CONVERTING TO POS-TARGS

To determine the relationship between observed dithers and POS-TARGs, we collected several dithered datasets and compared the executed offsets between images (in terms of the offset in distortion-corrected space between the frames) with the commanded POS-TARGs (given in arcseconds). The datasets we examined are listed in Table 1.

Table 1: List of datasets used to determine the relationship between the observed dithers and commanded POS-TARGs.

N	DATASET	PID	DATE	PA_V3	TARGET
01	icmz01	13809	23/02/2015	89.9998	WESTERLUND 1
02	icmz01	13809	23/02/2015	89.9994	WESTERLUND 1
03	iabi01	11445	23/07/2009	109.4500	47 TUC
04	ic9i04	13417	30/03/2014	87.2512	47 TUC
05	ibbw04	11931	13/03/2010	350.4230	47 TUC
06	ibcj01	11928	10/12/2009	86.0026	OMEGA CEN
07	ibcj04	11928	21/03/2010	149.0012	OMEGA CEN
08	ibcj07	11928	03/09/2010	312.9982	OMEGA CEN
09	iblq01	12340	30/05/2011	241.9976	OMEGA CEN
10	icnw34	13691	30/04/2015	227.1688	OMEGA CEN

For each dataset, we have a list of (Δu, Δv) offsets between each frame and the first frame paired with a list of (ΔPT_X, ΔPT_Y) offsets. For each set, we then fit the pairs with a linear relationship:

$$\begin{bmatrix}\Delta u\\ \Delta v\end{bmatrix} = \begin{pmatrix} A & B\\ -B & A\end{pmatrix}\begin{bmatrix}\Delta PT_X\\ \Delta PT_Y\end{bmatrix}$$

where A and B are the linear-transformation coefficients. Since both frames are presumed to be distortion-free, we expect there to be no linear skew so that there are only two terms: the scale and orientation. Figure 3 shows the solved-for values of A and B from the 10 datasets that we examined

The average value for A is 8.625 and that for B is 0.025. The value of A represents the plate-scale along y, meaning that there are 8.625 pixels per arcsecond, or 0.1159 arcseconds per pixel. The non-zero value

for *B* reflects a slight orientation difference (0.2°) between the *y* axis in our solution and that of the POS-TARG *y* axis.

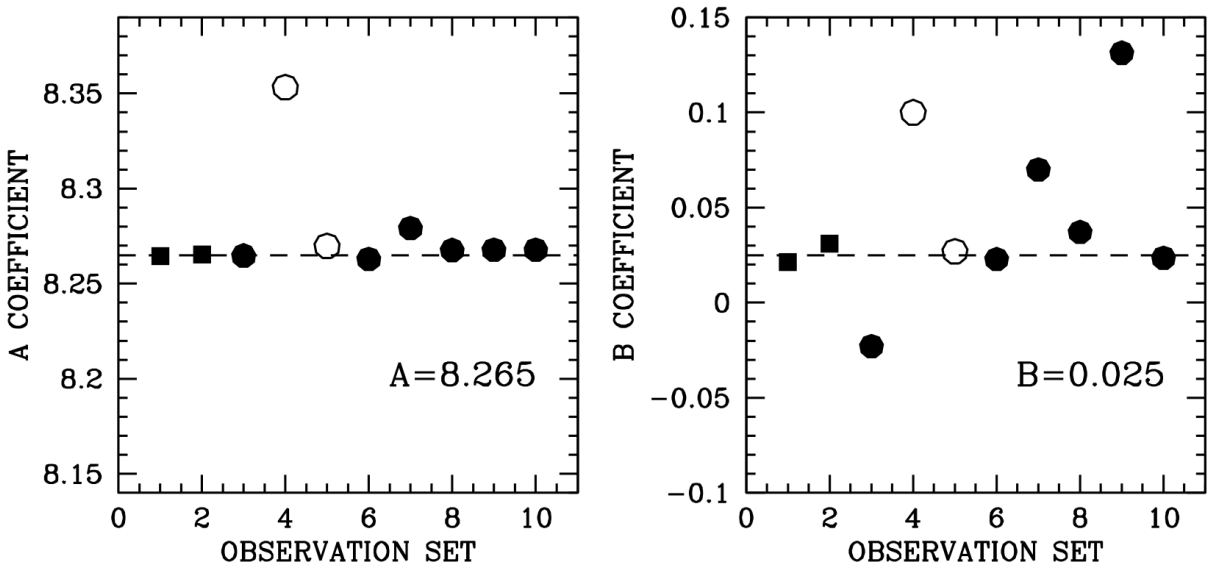

Figure 3: The solved-for linear-transformation coefficients relating the distortion-corrected system to the POS-TARG system. Each point represents the solved-for coefficients for a given data set. The filled circles are centered on the target and have large dithers. The open circles are centered and have small dithers. The filled squares are off-center, but have large dithers.

It is clear that there is much more scatter in B than in A. This is a reflection of the fact that the orientation of the telescope is not maintained perfectly during the visit. From the image headers, we see that the orientation typically varies by about 0.1° within a visit, which can explain much of the scatter we see in the right panel of Figure 3. This roll uncertainty will introduce some fundamental uncertainty into our ability to dither accurately with respect to pixel-phase when the dither steps are large. Like the pixel-phase error that comes from distortion, this error is also proportional to the amplitude of the dither offset. The pixel-phase decoherence related to roll uncertainty (0.01/8.625 ~ 0.1%) is about half as large as that introduced by distortion (0.2 pixels over 10 pixels, from Figure 1).

In addition to small changes in roll, Dressel (2012) notes that during the course of an orbit, the PSF typically drifts on the detector by up to ~8 mas (8% of a WFC3/IR pixel) in each coordinate. Guide-star re-acquisitions introduce offsets of 5 to 20 mas (RMS) when dither patterns cannot be completed within one orbit (DrizzlePac Handbook Apendix B). Thus, it is worth keeping in mind that even when we have a perfect dither pattern, the telescope does not always execute it perfectly. That said, the closer to perfect the pattern is, the more it can tolerate small errors in pointing without resulting in redundant and imbalanced pixel-phase coverage.

3.3 Validation of Our Model with Real Observation

To double-check our dither to POS-TARG relationship, we will examine a dataset that was taken with a dither that was carefully tailored to provide the best possible sub-pixel sampling. The data set is ic9i04 and it was taken for program 13417 (PI: Bennett) for the purpose of fitting for the separation between two stars that were part of a gravitational lensing event. A good dither was critical to allow the best possible estimate of the separation between the stars.

In constructing the Phase II plan for the original program, we divided the orbit into eight 300s exposures through F125W and dithered to get good pixel-phase sampling. Table 2 shows the image name and the POS-TARG executed for that exposure in the first three columns. The next two columns report the raw X and Y locations of the same star in each exposure from a fit with a library PSF (see Anderson 2016). The instrumental magnitude is given in the sixth column and indicates that the star is measured with an RMS of about 0.01 magnitude. The last two columns show where the above procedure says the star should be, based on its position in the first exposure, the input POS-TARG, the distortion solutions, and our model.

Table 2: List of images used in a 8-point dither and the input POS-TARGs and observed positions for a star near the center of the detector.

IMAGE_NAME	POS-TARGx	POS-TARGy	OBS_X	OBS_Y	OBS_M	MOD_X	MOD_Y
ic9i04idq	0.00000	0.00000	611.003	484.382	-9.093	611.003	484.382
ic9i04ifq	0.61181	-0.00001	615.517	484.346	-9.090	615.524	484.360
ic9i04ihq	0.30681	0.27324	613.302	486.590	-9.077	613.264	486.632
ic9i04ijq	0.91864	0.27326	617.819	486.590	-9.078	617.784	486.610
ic9i04ilq	0.00178	0.54654	611.039	488.886	-9.090	611.003	488.904
ic9i04inq	0.61365	0.54653	615.582	488.895	-9.087	615.524	488.882
ic9i04ipq	0.30862	0.81985	613.338	491.215	-9.075	613.264	491.154
ic9i04irq	0.92052	0.81987	617.851	491.194	-9.090	617.784	491.132

These data are shown graphically in Figure 4. It is clear that our POS-TARG-to-dither model does a good job predicting the achieved offsets, but the prediction is not perfect. Recall that Figure 3 showed that there is some variation in the dither-to-POS-TARG orientation and from Dressel (2012) we do expect small errors in pointing, so it is not surprising that the correspondence is not perfect. Even so, we clearly have a good enough model to construct a dither pattern that can provide a good 8-point dither across nearly 10 pixels.

Figure 5 shows what happens to the pattern when we examine a star in the corner of the detector. Since the pattern is contained within about 6×6 pixels, the pixel-phase drift isn't terrible, but it is clear that the sampling is less uniform at the corner than at the center (shown in Figure 4).

Now that we have a way to convert raw-detector dithers into POS-TARGs, we are now in a position to both evaluate and prescribe dither patterns. In the next section, we will evaluate the dithers provided in the Instrument Handbook. After that, we will come up with some additional patterns that users can consider for their programs.

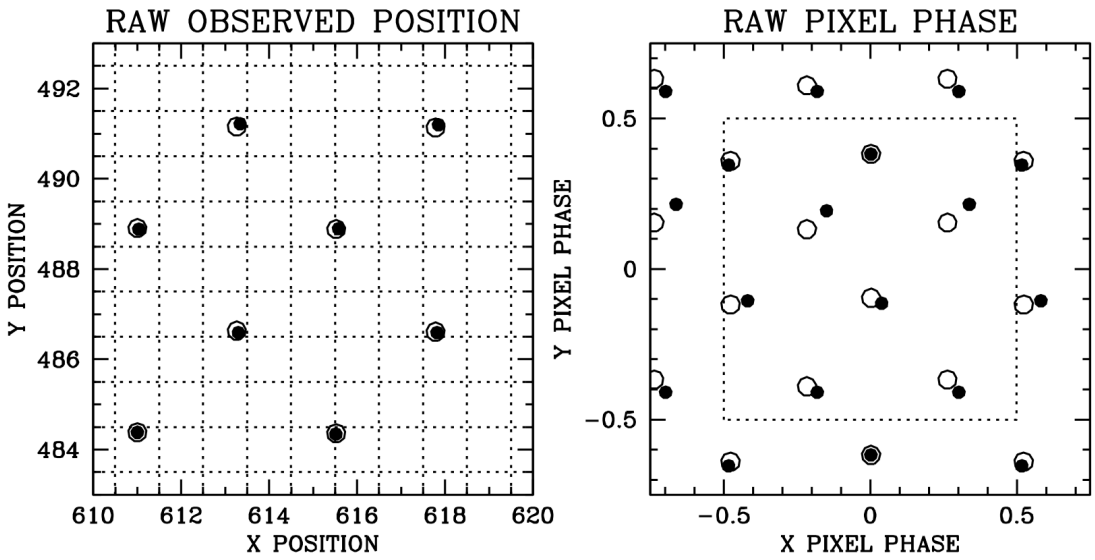

Figure 4: Data in Table 2 shown graphically. On the left, we show the observed location of a bright star in the eight dithered exposures in solid and the predicted position for the star based on the POS-TARGs and our model in the open circles. On the right, the same thing, but in terms of pixel phase.

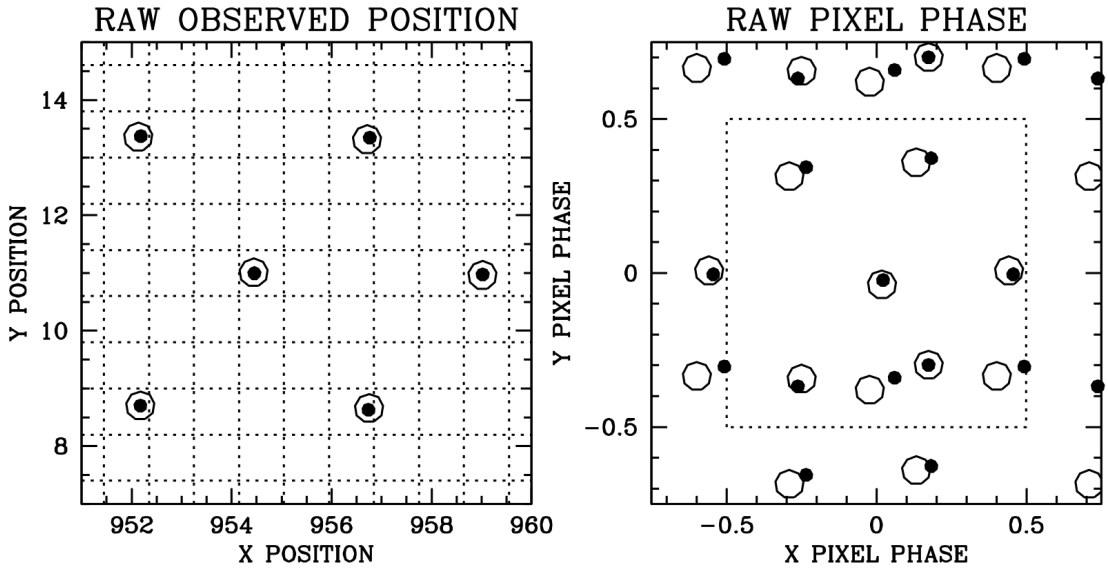

Figure 5: This is similar to Figure 4, but for a star in the lower-left corner of the detector. The sampling at the bottom of the pixel (drawn in as a dotted box) is much denser than at the top of the pixel, reflecting the pixel-phase drift that occurs in the presence of whole-pixel shifts and distortion.

4. EVALUATING THE RECOMMENDED DITHERS

We can use the mechanism described above to evaluate the dithering options provided in the Instrument Handbook. In Figure 6, we show the three options recommended for sub-pixel WFC3/IR dithering in the Instrument Handbook (see Appendix C3). The raw dither is shown on the left, the pixel-phase offset achieved is shown in the middle panel, and the input POS-TARGs are listed on the right. In the left and middle panels, we show the dither as achieved at the center of the detector by the solid blue dots, and in lines we show the impact of distortion on the achieved dither in terms of how the sub-pixel sampling shifts with respect to the point in the dither pattern at the corners of the field.

The fact that the two-point dither is only three pixels in total offset means that distortion does not have a large impact on the achieved pixel-phase coverage. The three-point dither, on the other hand, involves a 6-pixel offset and as such has considerable decoherence in the pattern achieved. In fact, the third point gets perturbed so much by distortion that it almost falls on top of the second point (in pixel phase) at some corners of the detector. We will come up with a three-point pattern in the next section that avoids this pitfall. The 4-point box pattern in the Handbook looks quite good, and the fact that there are at most 4 pixels total offset means that the pattern is quite coherent across the detector. It would be hard to improve on this.

Along with a comprehensive discussion of dithering strategies, Dahlen, Dressel, and Kalirai (2010) also provide suggestions for a 6-point pattern and an 8-point pattern. Their patterns are suggested in terms of crossing the 2-point pattern with the 3- and 4-point patterns, and can be converted into the POS-TARGs (Linda Dressel, personal communication), and are shown in Figure 7. Not surprisingly, the 6-point pattern has considerable pixel-phase decoherence at the edge of the field, since it is made up of the 3-point pattern. The 8-point pattern is better, but it also suffers at the edge of the field. Furthermore, the left panel shows that there is not much separation between the individual dithers, and as a result, they will not be as good at mitigating artifacts.

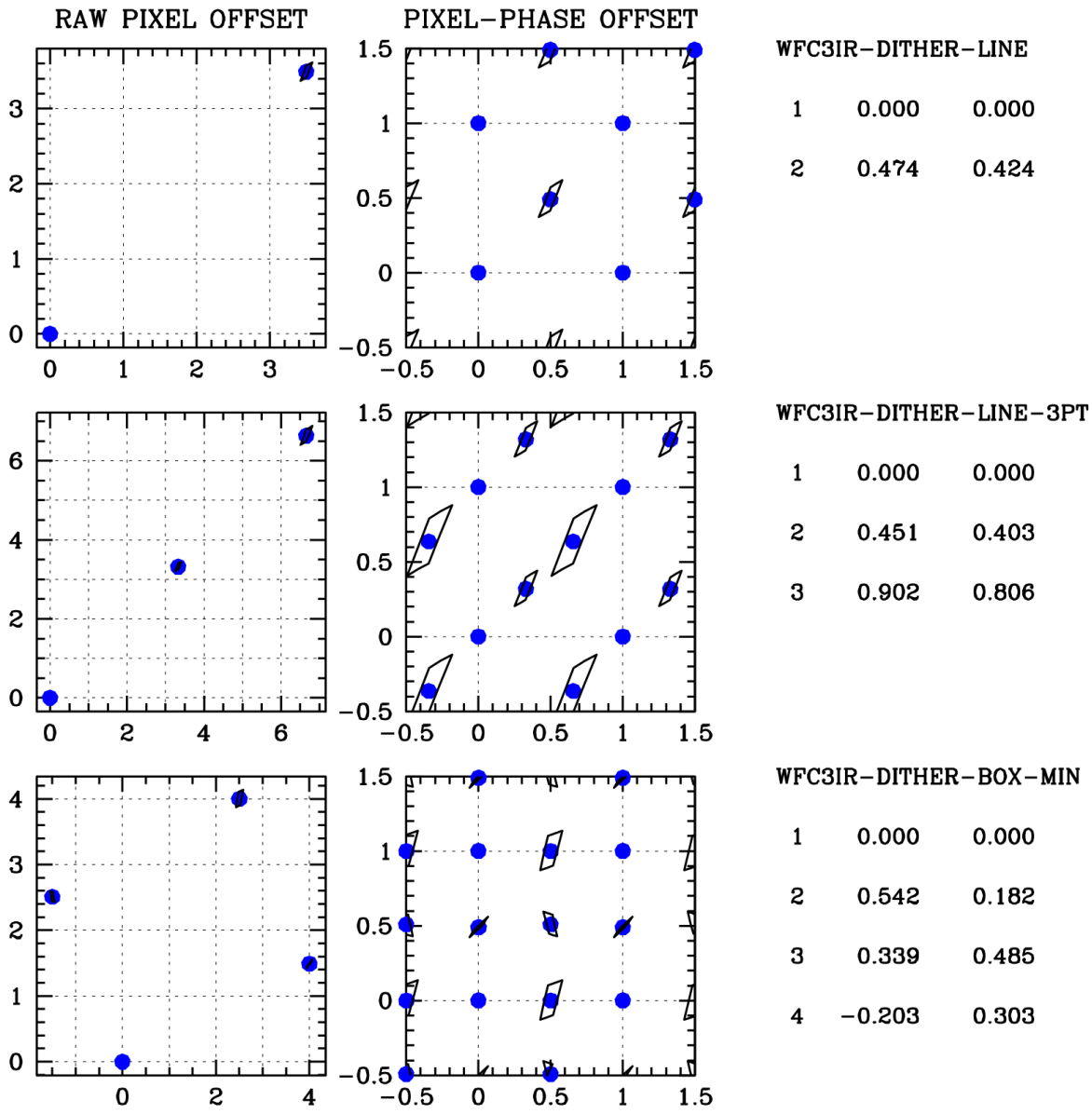

Figure 6: The 2-pt, 3-pt, and 4-pt dithers recommended in the Instrument Handbook. In the left panel we show the dither offsets with respect to a star at the center of the detector (507, 507) in the first exposure. The middle panel shows the achieved pixel phase. The solid point is the phase at the center of the detector, while the black outline shows the phase (relative to the first pointing) at the edges and corners of the detector.

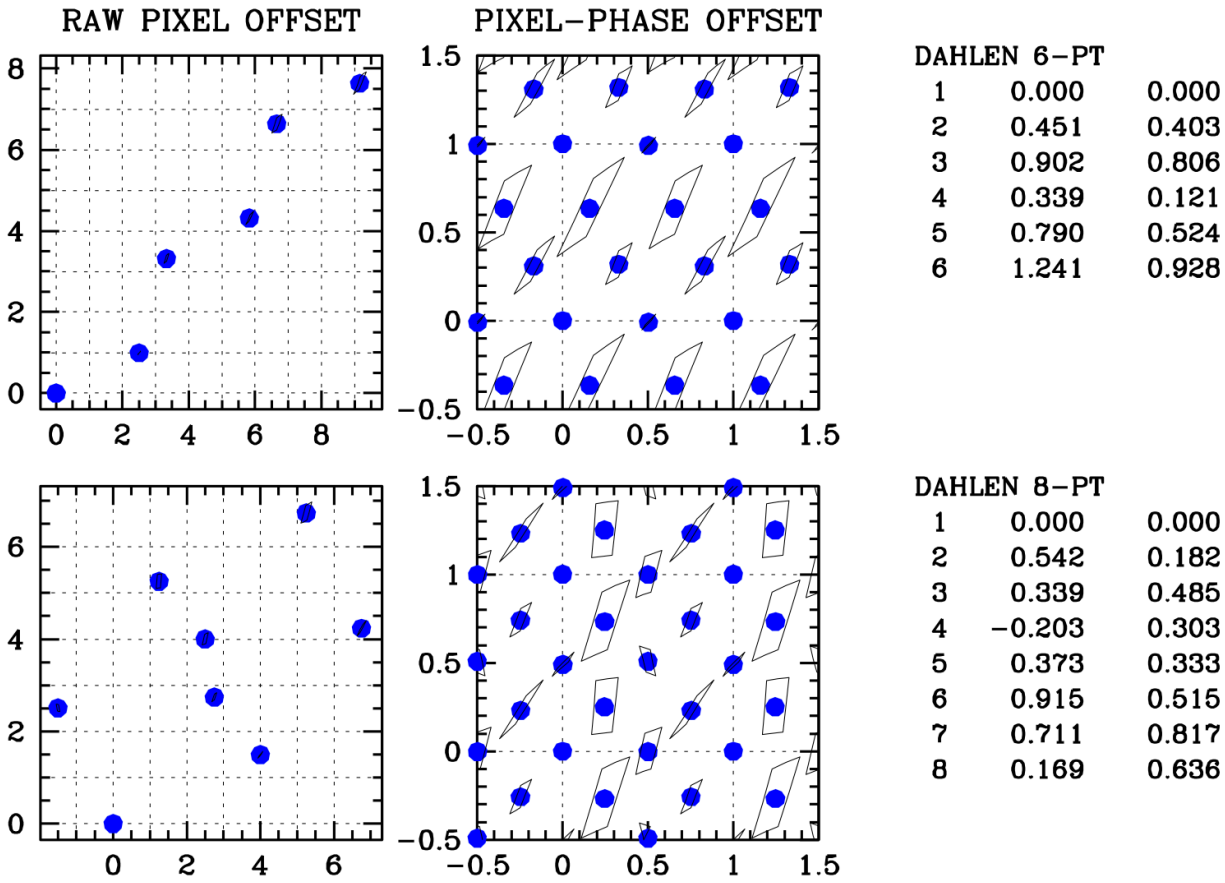

Figure 7: We evaluate two additional patterns provided in the WFC3/IR literature. These two come from Dahlen, Dressel, and Kalirai (2010); see Figure 6 caption for a description.

5. SOME ADDITIONAL DITHERS FOR FULL-FRAME TARGETS

The dither patterns evaluated in the previous section were designed to be good for the entire detector. We saw above that if we want the pixel phases to remain coherent even at the edges and corners of the detector, the entire dither pattern must span less than 5 pixels. To some extent this limits our ability to mitigate artifacts, since dithering by a couple pixels is not always as much as we would like to ensure that a multi-pixel artifact will affect a given object in only one exposure. We try to have our dithers separated by a minimum of two pixels in these "TIGHT" patterns. Figures 8 and 9 show the dithers we that have constructed for 3, 5, 6, 7, 8, and 9 points.

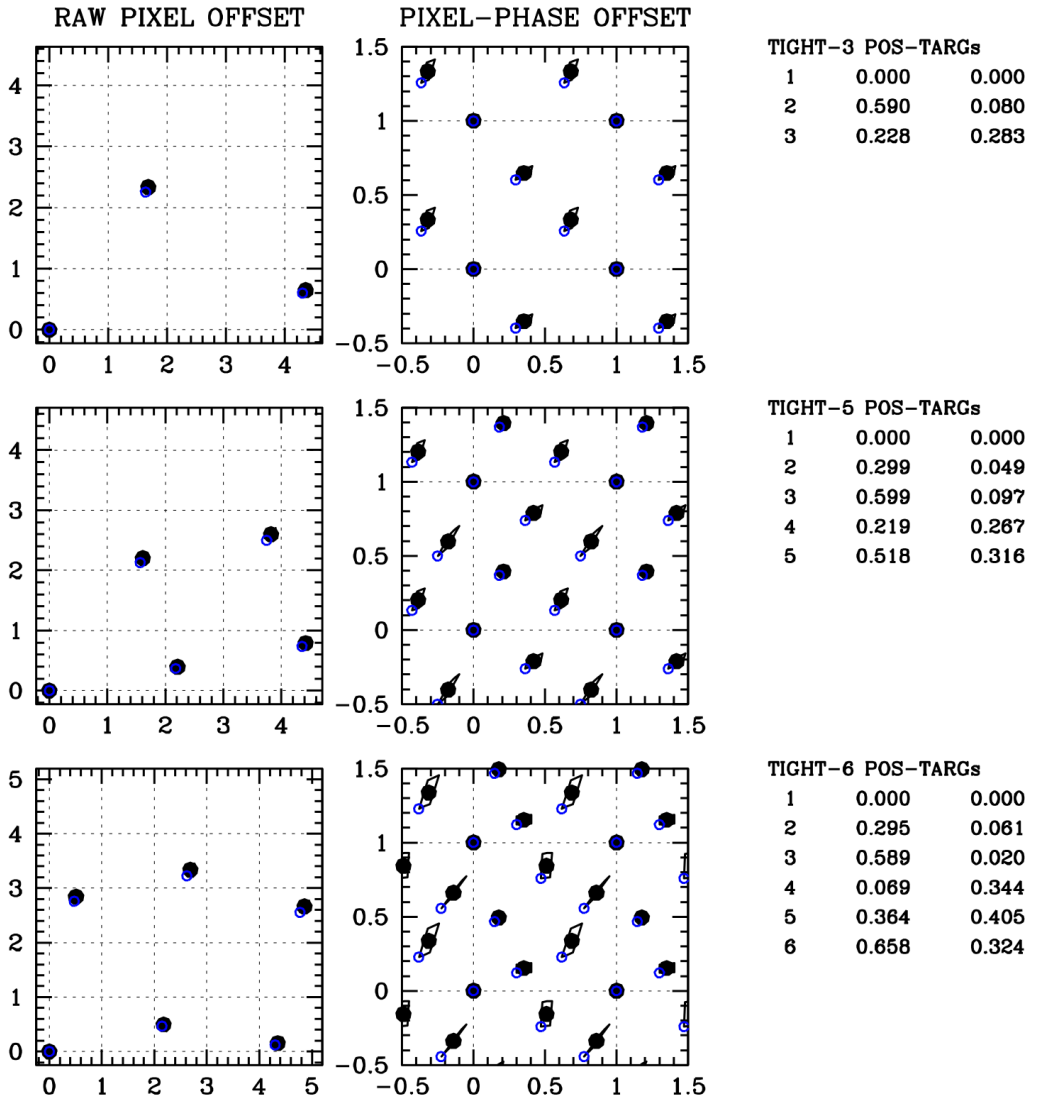

Figure 8: This presents the tight dither patterns for 3 points, 5 points, and 6 points. The solid black dot corresponds to the dither achieved at the center of the detector, the open circle to that at the upper-right corner, and the solid lines show all the corners. The dotted lines show the outlines of the pixels. The left panel shows the actual raw-pixel dithers and the middle panel shows the corresponding sub-pixel dithers. The POS-TARGs for input into APT are provided on the right.

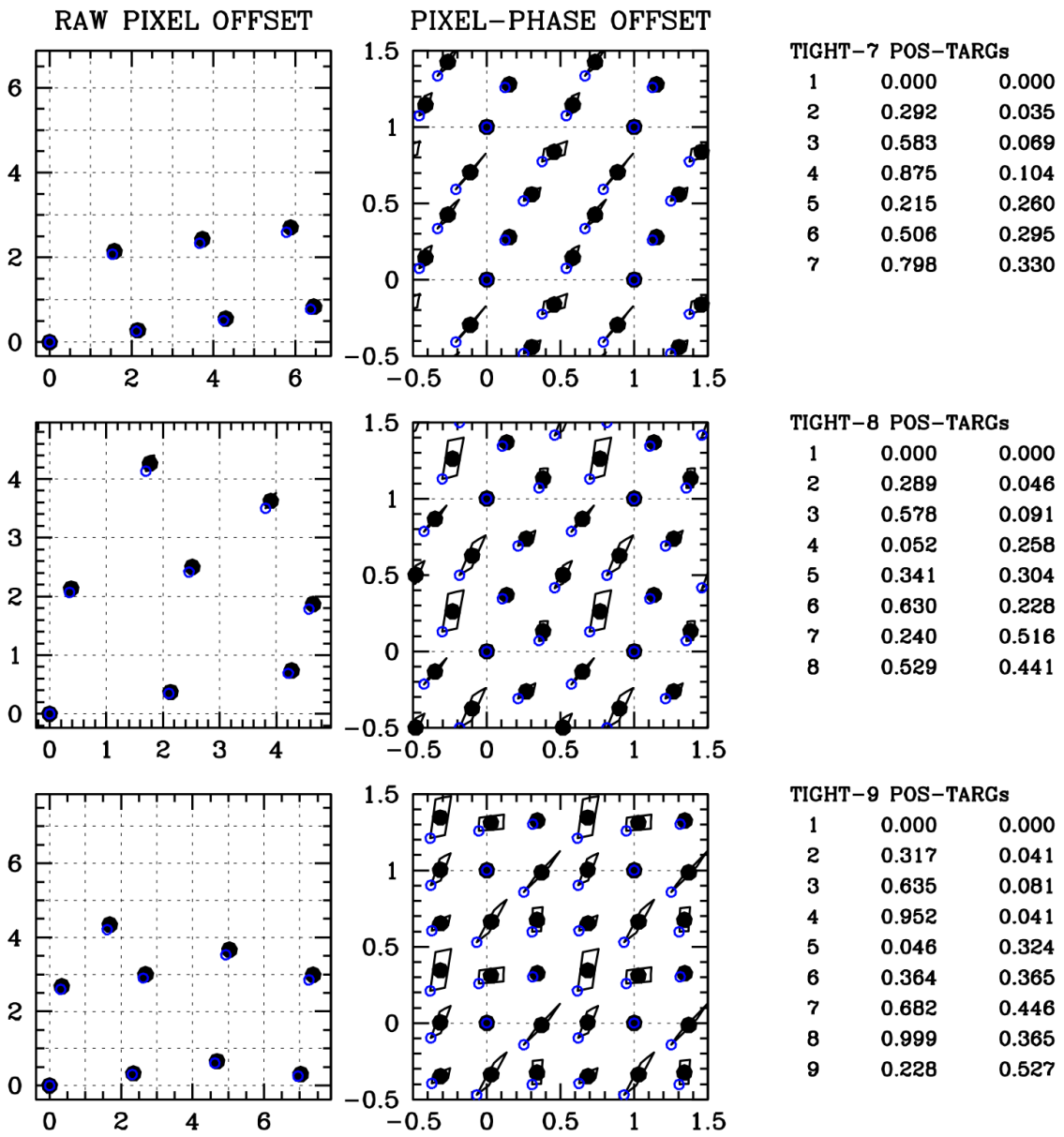

Figure 9: This presents the tight dither patterns for 7 points, 8 points, and 9 points in the same format as Figure 8.

The pattern provided in Figure 8 for a 3-point dither has the advantage over the one from the Handbook shown in Figure 6 that it is more compact in whole-pixel offset and therefore more coherent across the detector. Note that we have spread the dithers out more in the *x* direction than in the *y* direction since Figure 2 indicated that there is more distortion along the *y* axis.

These "TIGHT" patterns are designed to be used on fields where the entire detector is of interest. This could involve a single target, such as a galaxy that takes up most of the detector, or it could involve a field (such as extragalactic background, a cluster of galaxies or a cluster of stars) where there will be objects of interest over the entire detector.

Since the whole-pixel offsets here are relatively small, it is possible that a single artifact could affect multiple observations of a given object. If there are many sources of interest in the field, the user may be happy to deal with a few objects being compromised by artifacts knowing that the vast majority of them are extremely well sampled in pixel phase. Also, if there are any particularly bright objects, then persistence from the early images could cause problems in the later images. These considerations should be taken into account when choosing these tight dither patterns.

6. ADDITIONAL DITHERS FOR SMALL TARGETS

If the science focus is more on a target or targets that are clustered near the center of the detector, then the decoherence of the sub-pixel dither at the edges of the detector may not be so important. The user may prefer to ensure both a good dither *and* good artifact mitigation for the central region of the detector. For this purpose, we provide the dither patterns in Figures 10 and 11. These "WIDE" dither patterns will also do a better job dispersing the impact of persistence within the set of data. It would be natural to use these patterns for subarrays; since the imaging-focused WFC3/IR subarrays are centered roughly on the center of the detector, the patterns provided here should be good for them as well.

7. COMBINING DITHER PATTERNS

The additional patterns developed here are designed to provide optimal sub-pixel dithering for programs that have between 3 and 9 similar exposures in a visit. Some programs may have more observations than this. It would be possible to put together patterns with even more pointings, but once we have achieved 3×3 supersampling, we have already fully captured all the information contained in the scene. There is no particular benefit to having an organized dither pattern that provides denser coverage.

In the case where there are more than 9 observations to take, we recommend using the above patterns multiple times, with POS-TARG steps in between them, so that a given artifact will affect at most one observation of a particular object. Even if the POS-TARG steps between dither clusters is much larger than the ~5 pixels that would ensure pixel-phase coherence, the dithers within a cluster should still be coherent, thus ensuring that the overall coverage is even. As an example, if there are 16 exposures, one could imagine putting together two 8-point dithers, offset by a POS-TARG of perhaps 2.0 arcsecond (to mitigate for blobs, which can be 10-15 pixels in size according to Pirzkal, Viana, and Rajan 2010).

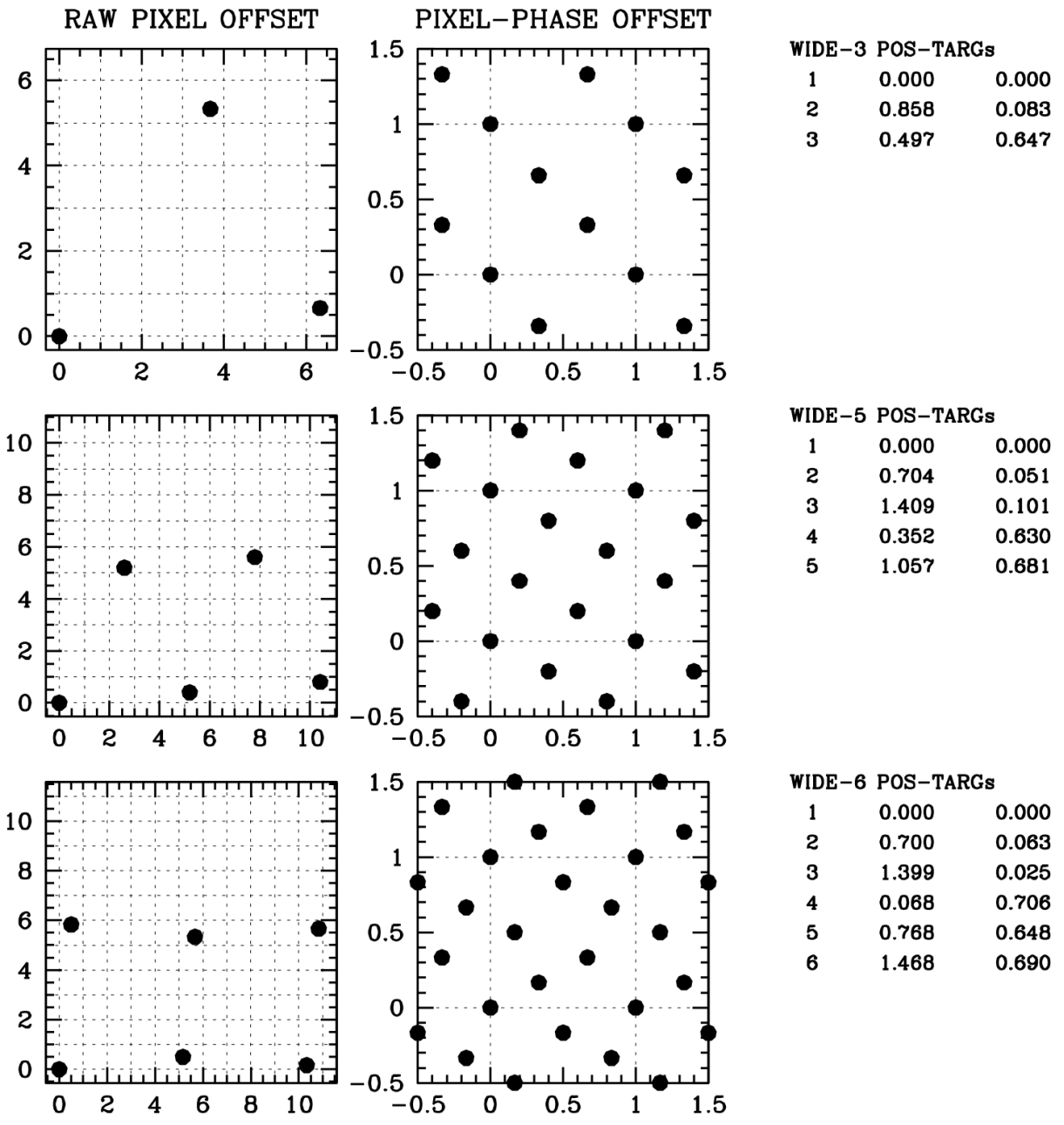

Figure 10: Similar to Figure 8, but the whole-pixel offsets between the dithers are larger, to do a better job mitigating artifacts. We do not show the impact of distortion on the pixel phase, as this pattern would become very incoherent at the edge of the chip. It is focused on the central half of the detector.

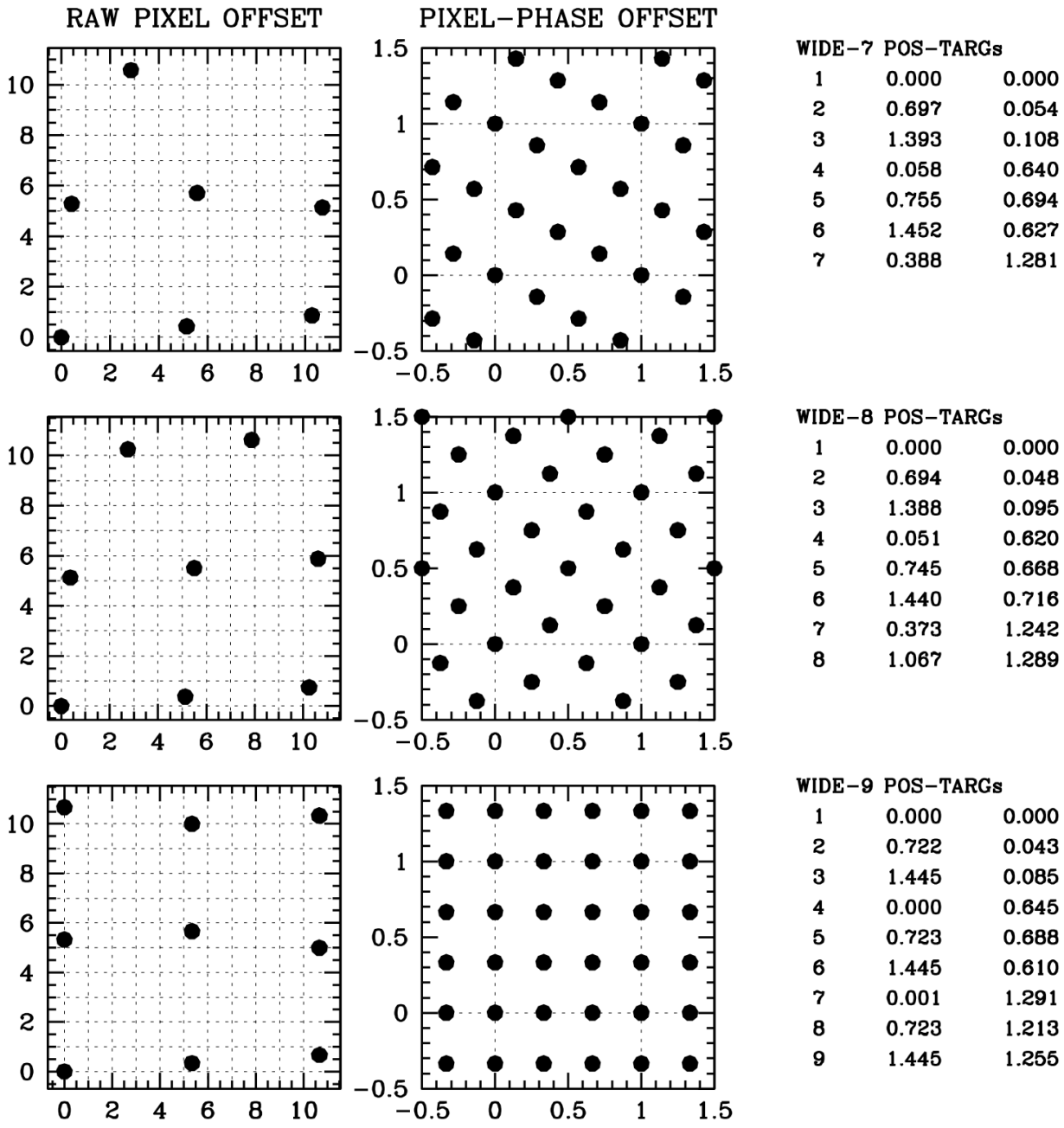

Figure 11: Similar to Figure 9, but the whole-pixel spacings between dithers is larger to allow better artifact mitigation.

8. CONCLUSIONS

Given the extremely undersampled nature of HST's WFC3/IR detector, dithering is an important consideration of most observing programs. We have developed a procedure for evaluating how geometric distortion affects the sub-pixel coverage of various dither patterns. We found that even a shift of just 6 pixels can cause significant decoherence of pixel-phase coverage. This means that there is often a trade-off between getting good pixel-phase coverage and mitigating the impact of detector artifacts.

We used the dither-evaluation procedure to examine the three patterns provided in the instrument handbook and find that the 2-point and 4-point patterns are quite good, but the 3-point pattern loses coherence at the edge of the detector. Since several programs would benefit from having a more comprehensive set of patterns, we have devised a set of patterns for N=3, 5, 6, 7, 8, and 9 steps for two cases: for the case where the whole detector is of interest and for the case where the target area is small. Users must enter the POS-TARGs explicitly by hand. There are currently no plans to implement them within APT.

I am grateful to Linda Dressel for her help in making this document possible, from her exploration of the cross patterns referred to in Dahlen et al (2010) to her careful reading of the evolving drafts, all of which helped to put this effort into a proper historical context and make it as useful as possible to WFC3/IR users.

REFERENCES

Anderson, J. 2016, WFC3/ISR 2016-12, *Empirical Models for the WFC3/IR PSF*

Dahlen, Dressel, and Kalirai, WFC3/ISR 2010-09, *Dithering Strategies for WFC3*

Dressel, L. 2012, WFC3/ISR 2012-14, *Breathing, Position Drift, and PSF Variations on the UVIS Detector*

Dressel, L. 2016. *Wide Field Camera 3 Instrument Handbook, Version 8.0* (Baltimore: STScI) http://www.stsci.edu/hst/wfc3/documents/handbooks/currentIHB

Pirzkal, N., Viana, A., Rajan, A. WFC3/IR 2010-06, *The WFC3 IR "Blobs"*